The metastable human brain associated with autistic-like traits

Authors: Takumi Sase[1,2,*], Keiichi Kitajo[1,3,4,*],

Affiliations:

1 Rhythm-based Brain Information Processing Unit, CBS-TOYOTA Collaboration Center, RIKEN Center for Brain Science, Wako, Saitama 351-0198, Japan

2 Department of Electrical Engineering, Faculty of Engineering, University of Malaya, Kuala Lumpur 50603, Malaysia

3 Division of Neural Dynamics, Department of System Neuroscience, National Institute for Physiological Sciences, National Institutes of Natural Sciences, Okazaki, Aichi 444-8585, Japan

4 Department of Physiological Sciences, School of Life Science, The Graduate University for Advanced Studies (SOKENDAI), Okazaki, Aichi 444-8585, Japan

*__Corresponding Authors (Equal Contribution)__:

Takumi Sase

CBS-TOYOTA Collaboration Center, RIKEN Center for Brain Science, Wako, Saitama 351-0198, Japan

E-mail: sase@brain.riken.jp

Keiichi Kitajo

CBS-TOYOTA Collaboration Center, RIKEN Center for Brain Science, Wako, Saitama 351-0198, Japan

Division of Neural Dynamics, Department of System Neuroscience, National Institute for Physiological Sciences, National Institutes of Natural Sciences, Okazaki, Aichi 444-8585, Japan

E-mail: kkitajo@nips.ac.jp

Conflict of Interest:

The authors declare no conflict of interest.

Acknowledgments:

This study was supported by a research grant from TOYOTA Motor Corporation. We are grateful to Ms. Yoko Noguchi for help with acquisition of EEG signals and AQ scores, and to Dr. Yuka O. Okazaki for helpful discussion.

Data and code availability:

All data and code related to the analyses and modeling in this study are available upon request.

Author contributions:

TS contributed to conceptualization, the development of methodology, detailed data analysis and modeling, software, writing the original draft, and review and editing. KK contributed to conceptualization, data acquisition, methodology, formal analysis, funding acquisition, review and editing, and supervision of the overall research.

Abstract

Recent studies suggest that the resting brain utilizes metastability such that the large-scale network can spontaneously yield transition dynamics across a repertoire of oscillatory states. By analyzing resting-state electroencephalographic signals and the autism-spectrum quotient acquired from healthy humans, we show experimental evidence of how autistic-like traits may be associated with the metastable human brain. Observed macroscopic brain signals exhibited slow and fast oscillations forming phase-amplitude coupling (PAC) with dynamically changing modulation strengths, resulting in oscillatory states characterized by different PAC strengths. In individuals with the ability to maintain a strong focus of attention to detail and less attention switching, these transient PAC dynamics tended to stay in a state for a longer time, to visit a lower number of states, and to oscillate at a higher frequency than in individuals with a lower attention span. We further show that attractors underlying the transient PAC could be multiple tori and consistent across individuals, with evidence that the dynamic changes in PAC strength can be attributed to changes in the strength of phase-phase coupling, that is, to dynamic functional connectivity in an electrophysiological sense. Our findings suggest that the metastable human brain can organize spontaneous events dynamically and selectively in a hierarchy of macroscopic oscillations with multiple timescales, and that such dynamic organization might encode a spectrum of individual traits covering typical and atypical development.

Keywords:

human brain dynamics, metastability, phase-amplitude coupling, autism spectrum

Significance Statement

Metastability in the brain is thought to be a mechanism involving spontaneous transitions among oscillatory states of the large-scale network. We show experimental evidence of how autistic-like traits may be associated with the metastable human brain by analyzing resting-state electroencephalographic signals and scores for the autism-spectrum quotient acquired from healthy humans. We found that slow and fast neural oscillations can form phase-amplitude coupling with dynamically changing modulation strengths, and that these transient dynamics can depend on the ability to maintain attention to detail and to switch attention. These results suggest that the metastable human brain can encode a spectrum of individual traits by realizing the dynamic organization of spontaneous events in a hierarchy of macroscopic oscillations with multiple timescales.

Introduction

The human brain can spontaneously yield transition dynamics across oscillatory states and organize a variety of events in a hierarchy of oscillations. Such spontaneous dynamics, particularly at rest, have been intensively observed and analyzed over many years, and attempts to model them have been made using dynamical systems theory, to achieve a better prediction of brain activity [1–5]. However, there is a lack of direct evidence that resting-state brain dynamics can originate from the underlying attractors, and little is known about the kind of attractors that may have functional roles in the dynamic organization of spontaneous activity in a way utilizing oscillatory hierarchy.

Electroencephalography (EEG) is a promising technique for the high temporal resolution observation of the dynamics of neural activity over large-scale brain networks. The observed macroscopic signals are oscillatory, such that the corresponding power spectrum can exhibit a single representative peak, and can be classified into multiple bands according to its frequency [6, 7]. The peak frequency of neural activity shows either a higher or lower value depending on brain function [6] and cognitive and behavioral performance [7]; for example, alpha-band activity can be enhanced or suppressed by attention, and its peak frequency can vary with age [7].

Observed macroscopic neural oscillations can reflect underlying nonlinear dynamics. Experimental studies have presented evidence that phase-phase coupling (PPC) allows phases detected from oscillations at a particular frequency to be coherent, thereby facilitating the nonlinear brain phenomenon called synchronization [8–10]. Furthermore, the phases have the ability to modulate the amplitude of a faster oscillatory component by forming phase-amplitude coupling (PAC) [11–15]. The PPC has been suggested to play a role in making functional connections among distant brain regions [8], while it is suggested that the PAC mediates computation between local and global networks [12], with both couplings having been observed in function-specific and individual behavior-related oscillations at multiple spatiotemporal scales [9, 14]. From a dynamical systems theory point of view, these two kinds of coupled oscillatory dynamics can be interpreted as being generated from coupled oscillatory attractors composed of the limit cycle [2] or its variant form, i.e., a torus in a high-dimensional phase space [16, 17]. These suggestions have inspired phenomenological modeling of the dynamics underlying EEG neural oscillations [18, 19], resulting in a variety of coupled nonlinear-oscillator systems that possess an essential property of brain dynamics, namely, the rhythm [20].

Oscillatory dynamics such as those mentioned above can make spontaneous transitions among multiple network states, particularly at rest. EEG signals observed during a resting condition can be labeled as a small number of states called microstates [21–24]. These microstates have been suggested to be associated with cognition and perception [22], as well as individual differences in brain function [24]. In recent years, resting-state EEG signals have been investigated from the point of view of functional connectivity of the large-scale network, which is often characterized by the strength of the PPC [25–27]. Betzel et al. showed that resting-state EEG phases can exhibit dynamic changes in PPC modulation, so that a repertoire of synchronized states of the large-scale network can appear [26]. Moreover, both EEG phases and amplitudes at rest were recently analyzed together [28, 29], because the PAC can also occur spontaneously [13]. These experimental findings imply that resting-state EEG phase dynamics not only exhibit synchronization, but that they also result in amplitude modulation at the same time via both PPC and PAC. Therefore, we developed the following hypotheses for the resting brain: (i) there is a repertoire of synchronous slow oscillations that interact via the PPC (Fig. 1A); (ii) these oscillations interact with fast ones via the PAC (Fig. 1B); (iii) this synchrony-dependent PAC can result in a repertoire of attractors characterized by slow and fast timescales (Fig. 1C); and (iv) transitions across attractors, i.e., dynamic changes in PAC strengths, can occur spontaneously at rest according to transitions among a repertoire of the synchronous slow oscillations, that is, according to the dynamic changes in PPC strengths (Fig. 1D).

In this study, we aimed to validate the dynamic PPC-PAC hypotheses described above (Fig. 1), and to show experimental evidence of how the metastable human brain is associated with autistic-like traits. In recent years, metastability in the brain has been proposed as a mechanism for integration and segregation across multiple levels of brain functions [30]. To elucidate aspects of the dynamics of the metastable human brain in this study, we first developed a method to label observed metastable dynamics as the underlying d-dimensional tori in a data-driven manner, under the assumption that these attractors can generate quasi-periodic oscillations such that slow oscillations can hierarchically modulate fast ones, following the oscillatory hierarchy hypothesis [31] (Materials and Methods). The method was then applied to 63-channel high-density scalp-recorded EEG signals from 130 healthy humans in an eyes-closed resting condition ($n = 162$ in total; 32 subjects participated in the experiment twice). The obtained results were compared with the autism-spectrum quotient (AQ) subscales [32,33] acquired from 88 of the subjects after the EEG recording, and were validated by a modeled coupled oscillator system driven by spontaneous fluctuations.

Results

The recorded brain dynamics, consisting of 63-channel scalp EEG signals from the resting human brain, were labeled as oscillatory states characterized by two peak frequencies, i.e., two-dimensional tori ($n = 101$), particularly as states with the alpha- and delta-band peak frequencies ranging from 8 to 12 Hz and 0.1 to 4 Hz, respectively ($n = 95$; Fig. 2, and Materials and Methods). The frequency of the fast oscillations was first estimated from the power spectra of the raw EEG signals (Figs. 2A and 2B; Fig. S1), and was used to calculate the corresponding instantaneous amplitudes (Fig. 2C). These amplitudes were still oscillatory around the frequency of the slow oscillations (Fig. 2D), and were thus converted further into corresponding instantaneous amplitudes (Fig. 2E) that did not show clear oscillations (Fig. 2F). A standard k-means clustering method with the Calinski-Harabasz criterion [34] was applied to these signals, and they were labeled as different strengths of the PAC (refer to Fig. 2G). These labeled signals (Fig. 2E) showed significant correlations with the time courses of the modulation index [13], with the significance level of the two-sided tests being corrected for multiple comparisons using the false-discovery rate (FDR) method [35] (FDR $p < 0.05$, in the scalp sites, accounting for more than 50 electrodes; see Fig. S2). The resulting dynamics obtained via two-time signal-to-instantaneous amplitude conversions were identified as a trajectory among the fixed points (zero-dimensional tori); namely, the original dynamics (Fig. 2A) were interpreted as a trajectory among tori with a dimension of two (Materials and Methods).

To more clearly demonstrate the two-dimensional tori as possible attractors for the resting human brain, we projected the obtained labeled signals (Fig. 2E) onto a lower-dimensional space (Fig. 3). We used a method of supervised dimensionality reduction called linear discriminant analysis (LDA) [36], which yields a space such that the projected trajectory can evolve into nearby points within each labeled state; this property is also consistent with the fixed point that can converge a trajectory into one point. The labeled signals were then projected onto a plane in the cases where the number of states was more than two (Figs. 3A and 3G), and were converted into a corresponding bivariate histogram (Figs. 3B and 3H); otherwise, the histogram would be a one-dimensional axis because of limitations of the LDA in this study. More specifically, we generated histograms with respect to each state using the same bin sizes and calculated the maxima of the counts of bins for each state, with these statistics then being regarded as the indices for the system's instability, which could be inversely proportional to the potential energy of the attractors. We tested whether the representative of the obtained statistics (the minimum in this study) was statistically significant, using the Fourier-transform (FT) surrogate for multivariate time-series data [37] under the null hypothesis H_0 where the labeled signals are linearly correlated Gaussian noise. We generated 200 surrogate data sets by shuffling phases of the labeled signals, applied these data to the k-means clustering, and projected the data with the obtained labels onto the same space as the original labeled signals (Materials and Methods). The surrogate data testing rejected H_0 for many individual data sets under the condition of $d = 2$ (FT test, one-sided $p < 0.05$, $n = 101$; Figs. 3C and 3I); none of these data sets were rejected under condition $d = 1$, and many were not rejected for $d = 0$ (FT test, one-sided $p>0.05$, $n = 162$ for $d = 1$ and $p>0.05$, $n = 99$ for $d = 0$; refer to Figs. D and J; the number of states was estimated with respect to each dimension d). The majority of the other data sets were rejected for $d = 3$ (FT test, one-sided $p < 0.05$, $n = 53$). As a whole, the surrogate data testing provided experimental evidence that macroscopic brain dynamics of the resting-state large-scale network can make spontaneous transitions across two- or three-dimensional tori. In particular, these attractors were characterized by two peak frequencies in the delta and alpha bands ($n = 95$), so that the states of the delta-alpha PAC can appear (Figs. 3E and 3K). We represented each state by a vector composed of mean values of the labeled signals (i.e. the delta-band instantaneous amplitudes depicted in Fig. 2E) over time, namely, by a 63-dimensional vector of mean PAC strengths.

Delta-alpha PAC states (Figs. 3E and 3K) were categorized into four groups across individuals ($n = 95$; Fig. 4). First, we converted these states into modified Z-scores [38] to standardize them robustly among individuals, with each data set being subtracted by the median and divided by the median absolute deviation instead of the mean and the SD, respectively, and all the data were subsequently multiplied by 0.6745 [38]. The obtained Z-scores were concatenated across states and individuals, and the resulting dataset was regarded as the data in a 63-dimensional feature space. In this space, we conducted principal component analysis (PCA) and applied a permutation test to 63 PCs by shuffling the dataset 200 times across the channel with respect to each component. The first four PCs significantly explained variance (one-sided, Bonferroni-corrected $p < 1.58 \times 10^{-4}$, total explained variance 81.6 %; Fig. 4A). Eigenvectors of these four PCs were then mapped as the topographies and categorized according to the regional distribution of the amplitude modulation in the occipital lobe, parietal lobe, and lateral and bilateral distributions in the occipital lobe (Fig. 4B).

The dynamics of transitions among the delta-alpha PAC states (Figs. 3F and 3L), as identified in this study, showed correlations with the two AQ subscores of ‘attention to detail’ and ‘attention switching’ ($n = 52$; Fig. 5). From the transition dynamics, we calculated the intervals between transitions (for which uncertain intervals at both edges were excluded) and obtained the following candidate statistics: the maximum, median, and minimum of the dwell time. These statistics, in addition to the number of states and the alpha- and delta-band peak frequencies estimated above, were regarded as test statistics (x) and were paired with the following five AQ subscores (y): social skills, attention to detail, attention switching, communication, and imagination. For these 30 pairwise statistics, we used multiple comparison tests with Pearson's correlation coefficients. The maximal dwell time showed a significant positive correlation with the attention-to-detail score ($r = 0.456$, two-sided, Bonferroni-corrected $p < 0.0013$; Fig. 5A, the effects of remaining variables in x on y were partially adjusted). Next, we conducted a post-hoc test of the multiple correlation coefficient using a linear regression model in which the attention-switching score was regarded as a dependent variable and was regressed against two statistics: the number of states and the alpha-band peak frequency (Fig. 5B), with these being selected because of weak significant correlations with the attention-switching score ($r = -0.283$, two-sided, uncorrected $p < 0.06$ for the number of states; and $r = 0.321$, two-sided, uncorrected $p < 0.03$ for the alpha-band peak frequency; Figs. 5C and 5D, the effects of the remaining variables in x on y were partially adjusted). The resulting linear combination showed significant correlation with the attention-switching score ($F\,(2, 49) = 4.91$, $r = 0.409$, $p < 0.006$), and factor loadings of this linear sum on the number of states and the alpha-band peak frequency (i.e. the correlation coefficients) were -0.614 and 0.666, respectively (Fig. 5B). The results indicated that in individuals with the ability to maintain a stronger focus on attention to detail and less attention switching, the delta-alpha PAC dynamics tended to stay in a particular state for a longer time, to visit a lower number of states, and to oscillate at a higher alpha-band peak frequency, thereby providing evidence on how autistic-like traits may be associated with the metastable human brain.

We modeled individual delta-alpha PAC dynamics ($n = 95$) to validate the dynamic PPC-PAC hypothesis (SI Text; Fig. 1). The model consisted of delta-band phases, alpha-band amplitudes, PPC-PAC connectivity, and fluctuations. We made connections among the delta-band phases, from delta-band phases to alpha-band amplitudes and from fluctuations to delta-band phases, such that synchronization, amplitude modulation, and state transition could occur via the PPC and PAC. The PPC connectivity and the level of fluctuations were estimated from the data for each individual (Fig. 6). On the other hand, the PAC connectivity was set to arbitrary values, because in the present model and our hypothesis, state transition can occur according to dynamic changes in PPC strengths (SI

Text; Fig. 1). Note that a part of the present model was composed of only delta-band phases, with the PPC being equivalent to the Kuramoto model subjected to noise (SI Text) [20].

First, we computed the current source density (CSD) [39, 40] from raw EEG signals to reduce the volume-conduction effect on the estimation of instantaneous phases, and then estimated the 'latent' phase attractors from the CSD signals (Figs. 6A and 6B; as shown later, the simulated delta-alpha PAC dynamics based on the CSD were converted back into EEG dynamics through observation, so that the modeling results would be consistent with the data analysis, see SI Text). Then, we converted the CSD signals into instantaneous phases around the delta-band peak frequency estimated from the data above, and labeled the obtained delta-band phases as multiple states by referring to the individual delta-alpha PAC dynamics (Figs. 3F and 3L). These labeled phases were further converted into the corresponding lags between every pair of phases, with their averages over time being calculated with respect to each labeled state (Fig. 6A). The resulting values were then transformed into phases for each state (Fig. 6B; SI Text), with these being regarded as attractors for the delta-band phase dynamics. In this study, we estimated these phase attractors from 19 CSD signals that corresponded with the standard 10/20 electrode system.

Next, we estimated the PPC connectivity underlying the delta-band phases and estimated the level of fluctuations (Figs. 6C and 6D; SI Text). Phase attractors estimated as described above were applied to the Kuramoto model composed only of delta-band phases, and they were converted into PPC connectivity (Fig. 6C; SI Text) [41]. We increased the level of fluctuations to phases in certain step sizes, simulated the corresponding models, and generated single realizations of the transitions for each level. The resulting set of transitions was quantified by the maximum, median, and minimum of the dwell time with respect to each fluctuation level, and from these statistics and those obtained from the data, we calculated the root-mean-square error (RMSE). We repeated this calculation 100 times and chose the fluctuation level minimizing the RMSE (Fig. 6D).

Then, we simulated the individual delta-alpha PAC dynamics ($n = 95$) as modeled above, and validated our dynamic PPC-PAC hypothesis (Fig. 7; SI Text). By calculating the overlaps [41] every time step (Figs. 7A and 7F; SI Text), we observed from the model that the strengths of the PPC changed dynamically among attractors, and that the alpha-band amplitudes were oscillatory at a frequency in the delta band, as well as the actual EEG data. These oscillatory amplitudes with a unit of CSD were first retranslated into those in the scalar potential, so that the modeling results would be consistent with the data analysis (SI Text), and were then converted into instantaneous amplitudes around a delta-band peak frequency, as estimated from the data above. Then, we labeled the resulting signals as delta-alpha PAC states by referring to the overlaps (Figs. 7A and 7F). The obtained labeled signals were projected onto a lower-dimensional space (Figs. 7B and 7G) and converted into corresponding histograms (Figs. 7C and 7H), which we used to conduct surrogate data testing in the same manner as for the data (Materials and Methods). For all simulated delta-alpha PAC dynamics, the surrogate data testing rejected H_0 under the condition of $d = 2$, but not under $d = 1$ (FT test, one-sided $p < 0.05$, $n = 95$ for $d = 2$ and $p>0.05$, $n = 95$ for $d = 1$; Figs. 7D, 7I, 7E, and 7J). Overall, we obtained consistent results from both the data and the model, providing evidence for the dynamic PPC-PAC hypothesis.

Finally, we attempted to predict the delta-alpha PAC dynamics with a temporally decreasing fluctuation level (Fig. 8). By calculating the overlaps every time step in this simulation, we observed that one of the delta-alpha PAC states was stabilized, so that the transition dynamics qualitatively changed into the dynamics in a steady state (Fig. 8A) as the fluctuation level decreased (Fig. 8B). The appearance of a steady state depended on the initial condition of the system. Moreover, such a qualitative change from multiple states to one state was viewed as a shrinking of the trajectory in the phase space (Fig. 8C). We generated the trajectories of the system under different initial conditions in a space composed of the overlaps. The trajectories were projected onto planes, from which we observed that the spaces filled by the transition dynamics can include the steady states as their subsets (Fig. 8C).

Discussion

In this study, we developed a data-driven approach to label observed metastable dynamics as the underlying d-dimensional tori. The method was applied to 63-channel scalp electroencephalographic (EEG) signals recorded from 130 healthy humans in an eyes-closed resting condition ($n = 162$ in total). The observed signals were labeled as tori with a dimension larger than one, such that PAC could occur hierarchically, in particular with a dimension of two, corresponding with the delta- and alpha-band peak frequencies ($n = 95$; Fig. 2). Then, the dynamics of the transitions among the delta-alpha PAC states (Fig. 3), which were categorized into four groups across individuals (Fig. 4), showed correlations with the autism-spectrum quotient (AQ) subscales of attention to detail and attention switching (Fig. 5). Finally, we qualitatively reproduced the obtained results in a coupled oscillator system driven by spontaneous fluctuations (Figs. 6 and 7) with some prediction (Fig. 8), to validate the hypothesis that the dynamic changes in PAC strengths can be attributed to changes in the strengths of PPC, that is, to dynamic functional connectivity in an electrophysiological sense (Fig. 1).

Many studies show that neural activity exhibits oscillations whose amplitudes change rhythmically over time [6, 12, 13, 42, 43]. A possible mechanism for this amplitude modulation is PAC, in which the phases of slow oscillations interact with the amplitudes of faster oscillations such that local and global computations in the large-scale network can cooperate [12, 13]; the PAC can take various forms depending on events such as visual and auditory tasks [42, 43]. In the present work, we identified a possible link of the PAC for resting-state EEG dynamics to the torus attractor, which is also characterized by slow and fast timescales (Figs. 1 and 2). Some modeling studies have shown evidence for a torus-related PAC [16, 17], such as the study of Sase et al., which analyzed a model composed of excitatory and inhibitory networks with dynamic synapses and revealed that amplitude-modulated dynamics can emerge from a trajectory into the torus or the closed curve, with these being mediated by bifurcation [16]. Hence, it is suggested that attractors in the resting brain can play a functional role in generating cooperative dynamics over the large-scale network and could be a torus, in which spontaneous events can be effectively processed by the utilization of multiple neural timescales.

A two- or three-dimensional torus was identified as a possible attractor underlying the resting-state EEG signals of most individuals (refer to Figs. 1 to 3). This result implies that macroscopic dynamics in the human brain can follow the oscillatory hierarchy hypothesis stating that slower and faster oscillations can interact hierarchically via the PAC [31, 44]. Lakatos et al. showed experimental evidence of EEG hierarchical organization: delta-band phases can modulate amplitudes of fast oscillations, which further make a spontaneous PAC connection to another faster oscillatory component [31]. We suggest that the resting human brain could utilize attractors with multiple timescales, so that a variety of events are spontaneously organized in a hierarchy of macroscopic neural oscillations.

Not only were the amplitudes of resting-state EEG signals rhythmic, but the strengths of the PAC (as obtained via two-time signal-to-instantaneous amplitude conversions) also exhibited dynamic changes such that transitions among multiple tori could occur (Fig. 3). Previous studies showed that the PAC strength can change dynamically over time, and transiently in response to sensory and cognitive events [12, 45–48]. Such dynamic coupling was observed during cognitive behavior in a T-maze task [45], learning [46], attentional allocation [47], and motor preparation [48]. Using a spatial-cuing task, Szczepanski et al. found PAC modulation-dependent attentional behavior in which the modulation strength was negatively correlated with the reaction time on a trial-by-trial basis [47]. Moreover, Kajihara et al. showed evidence that delta-alpha PAC can dynamically occur to mediate the global-to-local computation in motor preparation, such that the delta-band synchrony can make a direct link with the alpha-band amplitudes via the PAC [48]. These results may be supported by the conventional view of the task-dependent PAC [42, 43]: Voytek et al. reported that fast oscillations were strongly coupled with a slow oscillatory component via PAC during a visual task, and that this coupling weakened during an auditory task so that PAC with another slow oscillatory component could occur [43]. In recent years, it has been suggested that dynamic PAC plays a role in modulating the dynamics of the large-scale network, doing so more effectively than coupling with static modulation [12].

To the best of our knowledge, our finding of dynamic PAC, as realized by the transition among the attractors, is the first experimental report of this phenomenon. Crucially, we identified the transitions among delta-alpha PAC states (Fig. 3), which were further categorized into four groups across individuals ($n = 95$; Fig. 4). Previous studies showed evidence from resting-state functional magnetic resonance imaging (fMRI) signals that large-scale subnetworks with different functional connectivity, termed 'resting-state networks', are consistent across individuals [49, 50], and that these can consist of the following components: the default model network, the executive control network, the salience network, the dorsal attention network, and networks related to auditory, sensorimotor, and visual functions [50]. In recent years, it has been suggested that such networks are linked to the underlying electrophysiological oscillations [51, 52]. With respect to each network, Mantini et al. showed correlations between slow fluctuations in the blood-oxygen-level-dependent (BOLD) signal and EEG power variations of different brain rhythms, including delta and alpha rhythms [51]. Moreover, Britz et al. identified four resting-state networks from BOLD signals combined with the transition dynamics of EEG scalp potentials [52], referred to as EEG microstates [21–24], and a previous study likewise showed four network modules that were highly consistent across subjects [49]. These results inspired attempts to detect the large-scale functional network using only EEG data [53]. Moreover, the regional specificity of PAC has also been reported [43, 47], as well as the lateralization of PAC strengths [47]. Thus, macroscopic neural oscillations with multiple timescales in the resting human brain, identified as the delta-alpha PAC states in this study, could be the electrophysiological signatures of resting-state networks.

Our main finding is the AQ-related behavioral correlates of delta-alpha PAC dynamics, namely, the correlation with the two AQ subscales of attention to detail and attention switching (Fig. 5). In fact, slower neural oscillations are suggested to be dynamically entrained by rhythmic input from external sensory events [12, 14, 54]. Lakatos et al. showed that delta-band oscillations can selectively entrain to the rhythm of attended visual and auditory stimuli, thereby providing evidence of the neural entrainment to attention by which the brain can encode task-relevant events into preferred delta-band phases [14]. On the other hand, alpha-band oscillations have been suggested to play an inhibitory role by effectively gating top-down processing [55]. Previous studies show that the alpha-band power can decrease in the hemisphere contralateral to attended visual stimuli, whereas it exhibits an increase in the ipsilateral hemisphere (refer to Fig. 4); this is evidence for attention-induced alpha-band lateralization that can gate the flow of top-down information into task-irrelevant regions [55, 56]. Alpha-band activity can be dominantly observed in the resting brain, in particular in the occipital region [7], and the alpha-band peak frequency can depend on age and cognitive performance [7], which can show inter-individual variability [57]. Moreover, a recent study reported atypical neural timescales for individuals with autism spectrum disorder (ASD) [58], on the basis of the fact that the heterogeneity of timescales in the brain could be a basis for functional hierarchy [59]. Watanabe et al. found shorter neural timescales in sensory/visual regions and a longer timescale in the right caudate for individuals with a higher severity level of ASD [58]. Together, it is suggested that attractors in the resting human brain can generate individual delta-alpha PAC dynamics that can selectively encode spontaneous events by utilizing attention. Individual macroscopic dynamics in the brain, as identified here, and which tend to stay in a state for a longer time, to visit a lower number of states, and to oscillate at a higher alpha-band frequency in individuals with a stronger preference for specific events (Fig. 5), might be a neural signature of the autism spectrum, covering both typical and atypical development.

Recently, atypical transition dynamics of the resting large-scale network were identified as ASD symptoms [60]. By applying energy-landscape analysis [61] to the fMRI signals of resting-state networks, Watanabe and Rees showed that neurotypical brain activity can transit between two major states via an intermediate state, and that the number of these transitions can be lower due to the unstabilization of the intermediate state for the individuals with a higher severity level of ASD [60]. Such dynamics-behavior associations were linked to functional segregation. In this study, we generated the energy-like landscape of resting-state EEG dynamics by utilizing dimensionality reduction of tori, so that the underlying oscillatory attractors could transform into the fixed points (Fig. 3), and found a similar dynamics-behavior association between the dwell time of delta-alpha PAC state transitions and the attention-to-detail AQ subscale (Fig. 5A). Hence, the individual delta-alpha PAC dynamics could be the electrophysiological signature of an atypical balance in functional organization.

What kind of mechanisms can underlie the dynamic PAC and enable transitions among attractors? One possible mechanism is the metastability (or called criticality in a similar sense) that is suggested to play a role in maintaining a dynamic balance of integration and segregation of brain functions across multiple spatiotemporal scales [4, 30, 62]. Such dynamic organization was fruitfully discussed from viewpoints of both models and experimental data by Tognoli and Kelso [30]. By introducing an extended Haken-Kelso-Bunz model [62] and actual neurophysiological and behavioral data [30], they illustrated that phase dynamics in the brain can utilize both tendencies of dwells to be in synchrony and escapes into non-synchronous patterns, and associated this fact with the abilities of the brain (integration and segregation) in the theory of coordination dynamics [30, 62]. Similar dynamics were previously observed in the resting-state neural signals of EEG [23, 25, 26], fMRI [63], and functional multineuron calcium imaging [64] aimed at generating a better mathematical model of individual brains [1–5, 16, 18–20, 65, 66]; there is ongoing debate whether spontaneous neural activity originates from a deterministic dynamical system [62] that may yield chaotic itinerancy [67], or our present standpoint, a random dynamical system driven by spontaneous stochastic fluctuations [68–70]. Together, it is suggested that individual delta-alpha PAC dynamics at rest (which could relate to previous studies reporting that delta-alpha PAC can occur in preparation for a task [48] and during decision making [42]) can utilize metastability to organize spontaneous events in a hierarchy of macroscopic oscillations with multiple timescales.

Here, on the basis of our dynamic PPC-PAC hypothesis, we posit that the dynamic changes in delta-alpha PAC modulation can be attributed to changes in delta-band PPC; namely, to the dynamic functional connectivity in an electrophysiological sense (Fig. 1). Dynamic functional connectivity is referred to as the functional connectivity of the large-scale network with dynamically changing temporal correlation [71], and has been regularly observed in resting-state fMRI signals with behavioral and cognitive relevance [63,72]. In a similar sense, resting-state EEG experiments show that the dynamics of the large-scale network can transit among a repertoire of synchronized states [8,25,26]. We applied this view to the large-scale network of slow oscillations, taking into account its neuromodulatory influences on a faster oscillatory component, and validated the resulting dynamic PPC-PAC hypothesis using an extended version of the Kuramoto model (see Figs. 1, 6, and 7). By analyzing a model of local networks with heterogeneity near the onset of synchrony, a relevant modeling study demonstrated that transient synchrony of the large-scale network can organize the routing of information flow [73]. Dynamic and transient delta-alpha PAC, as identified in this study, may originate from the coupling between delta-band phases utilizing transient synchrony.

Finally, we observed shrinking of the transient PAC dynamics with a temporally decreasing fluctuation level from the model (Fig. 8). This result could relate to the reduction in trial-to-trial variability of cortical activity that can occur after the stimulus onset, such that the spontaneous and task-evoked brain activity can interplay in a complex manner [74]. Such a phenomenon was previously observed from the spikes of single neurons [75], and was recently demonstrated by a model including local and global cortical networks at multiple spatiotemporal scales [76]. Thus, the present model combined with the resting-state EEG data could have the potential for predicting task-relevant events; for example, identifying a parameter that can facilitate a dynamic balance in the typical and atypical neural activity of the large-scale network, which might be helpful for mitigating the severity level of ASD, so that faster transition dynamics among more states can appear during rest.

Taken together, we reported the first experimental evidence that (i) attractors in the resting human brain can be two- or three-dimensional tori; (ii) that their dynamics can be metastable delta-alpha PAC dynamics; and (iii) their functional role is associated with autistic-like traits. We suggest that the metastable human brain can organize spontaneous events dynamically and selectively in a hierarchy of macroscopic oscillations that interact in a cooperative manner, and that such dynamic organization might encode a spectrum of individual traits covering both typical and atypical development. Our findings on the metastable human brain and its association with autistic-like traits may be further corroborated by the following research: (i) the brain of ASD subjects during rest [60, 77, 78] to verify our present findings from healthy subjects; (ii) the brain during transcranial magnetic stimulation [29, 79] and closed-loop control by neurofeedback [56] to manipulate individual traits; and (iii) the brain during a task to understand the relationship between spontaneous and task-evoked dynamics from the viewpoint of the attractors that might underlie the human brain [74].

Materials and Methods

Data Acquisition

In total, 130 healthy humans participated in the EEG experiment after giving written informed consent. The EEG study was approved by the ethics committee of RIKEN and was conducted in accordance with the code of ethics of the Declaration of Helsinki. Thirty-two subjects participated in the experiment twice. The EEG signals were recorded from an EEG amplifier (BrainAmp MR+, Brain Products GmbH, Gilching, Germany) and a 63-channel EEG cap (Easycap, EASYCAP GmbH, Herrsching, Germany) placed on the scalp in accordance with the international 10/10 system with a left earlobe reference and AFz as a ground electrode. The signals were recorded for 180 s with the subjects in an eyes-closed resting condition. The following experimental configuration was used: sampling frequency 1000 Hz, low-cut frequency 0.016 Hz, and high-cut frequency 250 Hz. The recorded signals were offline re-referenced to the average potentials of the left and right earlobes. After the EEG experiment, 88 subjects were asked to answer the Japanese version of the AQ questionnaire [33], which was originally constructed by Baron-Cohen et al. (2001) [32]. The following five AQ subscales were scored from the obtained answers: social skills, attention to detail, attention switching, communication, and imagination. Our proposed method, named metastable states clustering, was applied to the raw EEG signals. All the analyses were conducted using in-house code custom written in MATLAB (Mathworks, Natick, MA, USA) with the EEGLAB [80], FieldTrip [81], and CSD

Toolboxes [39].

Metastable States Clustering

Metastable states clustering is a novel method that can label observed metastable dynamics as the underlying attractors, was developed in a data-driven manner. The method consists of the following three analyses: (i) dimensionality reduction of the tori, (ii) k-means clustering, and (iii) supervised dimensionality reduction of space. Analysis (i) was motivated by the Poincaré section in flow and sections in map [82] with their application [16]. We posited the following two assumptions: (I) the underlying attractors are d-dimensional tori and generate quasi-periodic oscillations with d peak frequencies $f_1, f_2, .., f_d$ that are rationally independent; and (II) these oscillations are amplitude-modulated such that slow oscillations with f_i can hierarchically modulate fast ones with f_{i+1} for $i = 1, 2, ..., d-1$, following the oscillatory hierarchy hypothesis [31]. We regarded d-dimensional tori with $d = 0$ and $d = 1$ as the attractors of fixed points and limit cycles respectively, and define here the following set: $\Omega_d = \{f_1, f_2, ..., f_d\}$.

Let $\boldsymbol{X}_{\Omega_d}(t)$ be N-dimensional data observed from the dynamics of transitions among K d-dimensional tori in a phase space at time t. In this study, we assumed $\boldsymbol{X}_{\Omega_d}(t)$ as the resting-state scalp EEG data with dimension $N = 63$, denoted by $\boldsymbol{X}_{\Omega_d}(t) = \left[X^1_{\Omega_d}(t), X^2_{\Omega_d}(t), ..., X^N_{\Omega_d}(t)\right]^{\mathrm{T}}$ for $t = 0$ to 180 s ($:= T$).

Analysis (i): Consider the observed dynamics $\boldsymbol{X}_{\Omega_d}(t)$ to be reduced to $\boldsymbol{X}_{\Omega_0}(t)$ (transitions among fixed points) via d-time iterations of a vector-valued function $\boldsymbol{F}: \mathbb{R}^N \to \mathbb{R}^N$ defined as

$$\boldsymbol{X}_{\Omega_{i-1}}(t) = \boldsymbol{F}\left(\boldsymbol{X}_{\Omega_i}(t)\right), \tag{1}$$

where $\boldsymbol{F} = [F_1, F_2, ..., F_N]^{\mathrm{T}}$. We realized $\boldsymbol{F}$ by recursively converting the signals into instantaneous amplitudes around frequency f_i, from $i = d$ to 1, and employed the complex-valued Morlet wavelet $\Psi_i(t)$ characterized by f_i and a parameter σ_i as follows [83]:

$$F_j\left(\boldsymbol{X}_{\Omega_i}(t)\right) = \left|\left(X^j_{\Omega_i} * \Psi_i\right)(t)\right|, \tag{2}$$

$$\Psi_i(t) = \sqrt{f_i}\exp\left(i2\pi f_i t\right)\exp\left(-t^2/2\sigma_i^2\right), \tag{3}$$

for $j = 1, 2, ..., N$. Operators $(\cdot * \cdot)$ and $|\cdot|$ denote a convolution and conversion from the complex value to its amplitude, respectively. To obtain the results at high temporal resolution, we set σ_i to a value such that the number of cycles n_{co} of the wavelet $\Psi_i(t)$ was three, i.e., $n_{\mathrm{co}} := 6f_i\sigma_i = 3$. We used data $\boldsymbol{X}_{\Omega_{i-1}}(t)$ for $t = n_{\mathrm{co}}/2f_i$ to $(T - n_{\mathrm{co}}/2f_i)$ to reduce the edge artifact of the wavelet $\Psi_i(t)$ with update $T - n_{\mathrm{co}}/f_i \rightarrow T$ with respect to each i. On the other hand, we estimated f_i from the power spectrum $P^j_{\Omega_i}(f)$ of $X^j_{\Omega_i}(t)$ for $j = 1, 2, ..., N$. We averaged these spectra over j with respect to each f, obtained a single spectrum, and estimated its peak frequency over the interval $1 \leq f < 45$ for $i = d$, otherwise in $0.1 \leq f < f_{i+1}$; for $i = d$ only, we first reduced the power-law effect on the spectrum $P^j_{\Omega_i}(f)$ which may follow $f^{-\beta_j}$ with a certain exponent [84] by simply subtracting the linear trend from $\log P^j_{\Omega_i}(f)$ vs. $\log f$.

Analysis (ii): Consider the dynamics $\boldsymbol{X}_{\Omega_0}(t)$ to be labeled as $L(t)$ via k-means clustering $G_K : \mathbb{R}^N \rightarrow \{1, 2, ..., K\}$. In this study, we estimated the number of states K by employing the Calinski-Harabasz index [34] in a condition of $K \in \{2, 3, ..., 10\}$. To obtain reproducible results, we initialized the clustering algorithm deterministically using PCA partitioning [85]. Note that we did not apply any kernel function to the present clustering analysis because the dynamics $\boldsymbol{X}_{\Omega_0}(t)$ appeared here can be a simpler representation of transitions among attractors in the phase space compared with $\boldsymbol{X}_{\Omega_d}(t)$.

Analysis (iii): Consider the labeled dynamics $\left(\boldsymbol{X}_{\Omega_0}(t), L(t)\right)$ to be converted into a lower-dimensional one $\boldsymbol{Y}(t)$ with dimension $n < N$ via projection $H : \mathbb{R}^N \times \{1, 2, ..., K\} \rightarrow \mathbb{R}^n$. In this study, we used LDA [36] to obtain $\boldsymbol{Y}(t)$ in a plane for the case of $K > 2$, otherwise in a one-dimensional axis due to limitation of the LDA. In this space, we generated histograms with respect to each labeled state $k \in \{1, 2, ..., K\}$ using the same bin sizes, and calculated the maxima of the counts of bins E_k for each k. The statistic

$E = \min_k E_k$ was applied to the FT surrogate data testing for multivariate time series [37] under the null hypothesis H_0, where $\boldsymbol{X}_{\Omega_0}(t)$ is linearly correlated Gaussian noise. We generated surrogate data $\boldsymbol{X}'_{\Omega_0}(t)$ by shuffling phases of $\boldsymbol{X}_{\Omega_0}(t)$, applied k-means clustering $G_K : \boldsymbol{X}'_{\Omega_0}(t) \mapsto L'(t)$, converted the labeled data $\left(\boldsymbol{X}'_{\Omega_0}(t), L'(t)\right)$ to lower-dimensional ones $\boldsymbol{Y}'(t)$ via the same projection H as $(\boldsymbol{X}_{\Omega_0}(t), L(t))$, and calculated the statistic E' of the surrogate data. We performed a one-sided test to verify whether E was significantly larger than E' by generating 200 surrogate data sets and setting the significance level to 0.05.

In summary, $\boldsymbol{X}_{\Omega_d}(t)$ was converted into $\boldsymbol{Y}(t)$ via the following composite function:

$$H\left(\boldsymbol{F}^d\left(\boldsymbol{X}_{\Omega_d}\right), G_K\left(\boldsymbol{X}_{\Omega_d}\right)\right). \tag{4}$$

For the case of $d = 0$ only, we first applied a band-pass filter to the raw EEG signals in a range between 1 and 45 Hz. It is expected that the proposed method can work efficiently under conditions where the data are recorded for a sufficiently long period with many sensors so that the observed dynamics and the actual dynamics can be one-to-one, and are less influenced by the observational noise arising from the experimental environment.

References

1. Deco G, Jirsa VK, Mclntosh AR (2011) Emerging concepts for the dynamical organization of resting-state activity in the brain. *Nat. Rev. Neurosci.* 12:43–56.

2. Cabral J, Kringelbach ML, Deco G (2014) Exploring the network dynamics underlying brain activity during rest. *Prog. Neurobiol.* 114(1):102–131.

3. Breakspear M (2017) Dynamic models of large-scale brain activity. *Nat. Neurosci.* 20(3):340–352.

4. Cocchi L, Gollo LL, Zalesky A, Breakspear M (2017) Criticality in the brain: A synthesis of neurobiology, models and cognition. *Progr. Neurobiol.* 158:132–152.

5. Cabral J, Kringelbach ML, Deco G (2017) Functional connectivity dynamically evolves on multiple time-scales over a static structural connectome: Models and mechanisms. *NeuroImage* 160:84–96.

6. Buzsáki G, Draguhn A (2004) Neuronal oscillations in cortical networks. *Science* 304(5679):1926–1929.

7. Klimesch W (1999) Eeg alpha and theta oscillations reflect cognitive and memory performance: a review and analysis. *Brain Res. Rev.* 29(2-3):169–195.

8. Varela F, Lachaux JP, Rodriguez E, Martinerie J (2001) The brainweb: Phase synchronization and large-scale integration. *Nat. Rev. Neurosci.* 2:229–239.

9. Doesburg SM, Roggeveen AB, Kitajo K, Ward LM (2008) Large-scale gamma-band phase synchronization and selective attention. *Cereb. Cortex* 18(2):386–396.

10. Hipp JF, Engel AK, Siegel M (2011) Oscillatory synchronization in large-scale cortical networks predicts perception. *Neuron* 69(2):387–396.

11. Jensen O, Colgin LL (2007) Cross-frequency coupling between neuronal oscillations. *Trends Cogn. Sci.* 11(7):267–269.

12. Canolty RT, Knight RT (2010) The functional role of cross-frequency coupling. *Trends Cogn. Sci.* 14(11):506–515.

13. Canolty RT, et al. (2006) High gamma power is phase-locked to theta oscillations in human neocortex. *Science* 313(5793):1626–1628.

14. Lakatos P, Karmos G, Mehta AD, Ulbert I, Schroeder CE (2008) Entrainment of neuronal oscillations as a mechanism of attentional selection. *Science* 320(5872):110–113.

15. Aru J, et al. (2015) Untangling cross-frequency coupling in neuroscience. *Curr. Opin. Neurobiol.* 31:51–61.

16. Sase T, Katori Y, Komuro M, Aihara K (2017) Bifurcation analysis on phase-amplitude cross-frequency coupling in neural networks with dynamic synapses. *Front. Comput. Neurosci.* 11(18):1–19.

17. Velarde OM, Urdapilleta E, Mato G, Dellavale D (2019) Bifurcation structure determines different phase-amplitude coupling patterns in the activity of biologically plausible neural networks. *NeuroImage* 202(15):1–20.

18. Ibáñez-Molina AJ, Iglesias-Parro S (2016) Neurocomputational model of eeg complexity during mind wandering. *Front. Comput. Neurosci.* 10(20):1–10.

19. Finger H, et al. (2016) Modeling of large-scale functional brain networks based on structural connectivity from dti: Comparison with eeg derived phase coupling networks and evaluation of alternative methods along the modeling path. *PLoS Comput. Biol.* 12(8):e1005025.

20. Breakspear M, Heitmann S, Daffertshofer A (2010) Generative models of cortical oscillations: neurobiological implications of the kuramoto model. *Front. Hum. Neurosci.* 11(190):1–14.

21. Lehmann D, Ozaki H, Pal I (1987) Eeg alpha map series: brain micro-states by space-oriented adaptive segmentation. *Electroencephalogr. Clin. Neurophysiol.* 67(3):271–288.

22. Britz J, Landis T, Michel CM (2009) Right parietal brain activity precedes perceptual alternation of bistable stimuli. *Cereb. Cortex* 19(1):55–65.

23. Ville DVD, Britz J, Michel CM (2010) Eeg microstate sequences in healthy humans at rest reveal scale-free dynamics. *Proc. Natl. Acad. Sci. U. S. A.* 107(42):18179–18184.

24. Schlegel F, Lehmann D, Faber PL, Milz P, Gianotti LRR (2012) Eeg microstates during resting represent personality differences. *Brain Topogr.* 25(1):20–26.

25. Ito J, Nikolaev AR, van Leeuwen C (2007) Dynamics of spontaneous transitions between global brain states. *Hum. Brain Mapp.* 28(9):904–913.

26. Betzel RF, et al. (2012) Synchronization dynamics and evidence for a repertoire of network states in resting eeg. *Front. Comput. Neurosci.* 6(74):1–13.

27. Kawano T, et al. (2017) Large-scale phase synchrony reflects clinical status after stroke: An eeg study. *Neurorehabil. Neural Repair.* 31(6):561–570.

28. Noda Y, et al. (2017) Resting-state eeg gamma power and theta-gamma coupling enhancement following high-frequency left dorsolateral prefrontal rtms in patients with depression. *Clinical Neurophysiol.* 128(3):424–432.

29. Glim S, et al. (2019) Phase-amplitude coupling of neural oscillations can be effectively probed with concurrent tms-eeg. *Neural Plast.* 2019(6263907):1–13.

30. Tognoli E, Kelso JAS (2014) The metastable brain. *Neuron* 81(1):35–48.

31. Lakatos P, et al. (2005) An oscillatory hierarchy controlling neuronal excitability and stimulus processing in the auditory cortex. *J. Neurophysiol.* 94(3):1904–1911.

32. Baron-Cohen S, Wheelwright S, Skinner R, Martin J, Clubley E (2001) The autism-spectrum quotient (aq): Evidence from asperger syndrome/high-functioning autism, malesand females, scientists and mathematicians. *J. Autism Dev. Disord.* 31(1):5–17.

33. Wakabayashi A, Baron-CohenSally S, Wheelwright S, Tojo Y (2006) The autism-spectrum quotient (aq) in japan: A cross-cultural comparison. *J. Autism Dev. Disord.* 36(2):263–270.

34. Caliński T, Harabasz J (1974) A dendrite method for cluster analysis. *Commun. Stat.* 3(1):1–27.

35. Benjamini Y, Hochberg Y (1995) Controlling the false discovery rate: a practical and powerful approach to multiple testing. *J. Roy. Statist. Soc. B* 57(1):289–300.

36. Fukunaga K (1990) *Introduction to statistical pattern recognition.* (Academic Press, Boston), 2nd edition.

37. Prichard D, Theiler J (1994) Generating surrogate data for time series with several simultaneously measured variables. *Phys. Rev. Lett.* 73(7):951–954.

38. Iglewicz B, Hoaglin DC (1993) *How to detect and handle outliers.* (WI: ASQC Quality Press, Milwaukee).

39. Kayser J, Tenke CE (2006) Principal components analysis of laplacian waveforms as a generic method for identifying erp generator patterns: I. evaluation with auditory oddball tasks. *Clin. Neurophysiol.* 117(2):348–368.

40. Perrin F, Pernier J, Bertrand O, Echallier JF (1989) Spherical splines for scalp potential and current density mapping. *Electroencephalogr. Clin. Neurophysiol.* 72(2):184–187.

41. Aoyagi T (1995) Network of neural oscillators for retrieving phase information. *Phys. Rev. Lett.* 74(20):4075–4078.

42. Cohen MX, Elger CE, Fell J (2009) Oscillatory activity and phase-amplitude coupling in the human medial frontal cortex during decision making. *J. Cogn. Neurosci.* 21(2):390–402.

43. Voytek B, et al. (2010) Shifts in gamma phase-amplitude coupling frequency from theta to alpha over posterior cortex during visual tasks. *Front. Hum. Neurosci.* 4(191):1–9.

44. Raichle ME (2011) The restless brain. *Brain Connect.* 1(1):106–113.

45. Tort ABL, et al. (2008) Dynamic cross-frequency couplings of local field potential oscillations in rat striatum and hippocampus during performance of a t-maze task. *Proc. Natl. Acad. Sci. U. S. A.* 105(51):20517–20522.

46. Tort ABL, Komorowski RW, Manns JR, Kopell NJ, Eichenbaum H (2009) Theta-gamma coupling increases during the learning of item-context associations. *Proc. Natl. Acad. Sci. U. S. A.* 106(49):20942–20947.

47. Szczepanski SM, et al. (2014) Dynamic changes in phase-amplitude coupling facilitate spatial attention control in fronto-parietal cortex. *PLoS Biol.* 12(8):e1001936.

48. Kajihara T, et al. (2015) Neural dynamics in motor preparation: From phase-mediated global computation to amplitude-mediated local computation. *NeuroImage* 118:445–455.

49. Moussa MN, Steen MB, Laurienti PJ, Hayasaka S (2012) Consistency of network modules in resting-state fmri connectome data. *PLoS ONE* 7(8):e4428.

50. Raichle ME (2015) The brain's default mode network. *Annu. Rev. Neurosci.* 38:433–447.

51. Mantini D, Perrucci MG, Gratta CD, Romani GL, Corbetta M (2007) Electrophysiological signatures of resting state networks in the human brain. *Proc. Natl. Acad. Sci. U. S. A.* 104(32):13170–13175.

52. Britz J, Ville DVD, Michel CM (2010) Bold correlates of eeg topography reveal rapid resting-state network dynamics. *NeuroImage* 52(4):1162–1170.

53. Liu Q, Farahibozorg S, Porcaro C, Wenderoth N, Mantini D (2017) Detecting large-scale networks in the human brain using high-density electroencephalography. *Hum. Brain Mapp.* 38(9):4631–4643.

54. Schroeder CE, Lakatos P (2008) Low-frequency neuronal oscillations as instruments of sensory selection. *Trends Neurosci.* 32(1):9–18.

55. Jensen O, Mazaheri A (2010) Shaping functional architecture by oscillatory alpha activity: gating by inhibition. *Front. Hum. Neurosci.* 4(186):98–113.

56. Okazaki YO, et al. (2015) Real-time meg neurofeedback training of posterior alpha activity modulates subsequent visual detection performance. *NeuroImage* 107:323–332.

57. Haegens S, Cousijn H, Wallis G, Harrison PJ, Nobre AC (2014) Inter- and intra-individual variability in alpha peak frequency. *NeuroImage* 92:46–55.

58. Watanabe T, Rees G, Masuda N (2019) Atypical intrinsic neural timescale in autism. *eLIFE* 8(e42256):1–16.

59. Himberger KD, Chien HY, Honey CJ (2018) Principles of temporal processing across the cortical hierarchy. *Neuroscience* 389:161–174.

60. Watanabe T, Rees G (2017) Brain network dynamics in high-functioning individuals with autism. *Nat. Commun.* 8(16048):1–14.

61. Ezaki T, Watanabe T, Ohzeki M, Masuda N (2018) Energy landscape analysis of neuroimaging data. *Philos. Trans. A* 375(2096):1–14.

62. Kelso JAS (2012) Multistability and metastability: understanding dynamic coordination in the brain. *Phil. Trans. R. Soc. B* 367:906–918.

63. Cabral J, et al. (2017) Cognitive performance in healthy older adults relates to spontaneous switching between states of functional connectivity during rest. *Sci. Rep.* 7(5135):1–13.

64. Sasaki T, Matsuki N, Ikegaya Y (2007) Metastability of active ca3 networks. *J. Neurosci.* 27(3):517–528.

65. Deco G, Kringelbach ML, Jirsa VK, Ritter P (2017) The dynamics of resting fluctuations in the brain: metastability and its dynamical cortical core. *Sci. Rep.* 7(3095):1–14.

66. Roberts JA, et al. (2019) Metastable brain waves. *Nat. Commun.* 10(1056):1–17.

67. Kaneko K, Tsuda I (2003) Chaotic itinerancy. *Chaos* 13:926.

68. Kitajo K, Nozaki D, Ward LM, Yamamoto Y (2003) Behavioral stochastic resonance within the human brain. *Phys. Rev. Lett.* 90(21):218103.

69. Kitajo K, et al. (2007) Noise-induced large-scale phase synchronization of human-brain activity associated with behavioral stochastic resonance. *Europhys. Lett.* 80(4):40009.

70. Sase T, Ramírez JP, Kitajo K, Aihara K, Hirata Y (2016) Estimating the level of dynamical noise in time series by using fractal dimensions. *Phys. Lett. A* 380(11–12):1151–1163.

71. Preti MG, Bolton TA, Ville DVD (2017) The dynamic functional connectome: State-of-the-art and perspectives. *NeuroImage* 160:41–54.

72. Cohen JR (2018) The behavioral and cognitive relevance of time-varying, dynamic changes in functional connectivity. *NeuroImage* 180:515–525.

73. Palmigiano A, Geisel T, Wolf F, Battaglia D (2017) Flexible information routing by transient synchrony. *Nat. Neurosci.* 20(7):1014–1022.

74. He BJ (2013) Spontaneous and task-evoked brain activity negatively interact. *J. Neurosci.* 33(11):4672–4682.

75. Luczak A, Bartho P, Harris KD (2009) Spontaneous events outline the realm of possible sensory responses in neocortical populations. *Neuron* 62(3):413–425.

76. Ponce-Alvarez A, He BJ, Hagmann P, Deco G (2015) Task-driven activity reduces the cortical activity space of the brain: Experiment and whole-brain modeling. *PLoS Comput. Biol.* 11(8):e1004445.

77. Yahata N, et al. (2016) A small number of abnormal brain connections predicts adult autism spectrum disorder. *Nat. Commun.* 7(11254):517–528.

78. Kawasaki M, et al. (2017) Frontal theta activation during motor synchronization in autism. *Sci. Rep.* 7(15034):1–8.

79. Kawasaki M, Uno Y, Mori J, Kobata K, Kitajo K (2014) Transcranial magnetic stimulation-induced global propagation of transient phase resetting associated with directional information flow. *Front. Hum. Neurosci.* 8(173):1–13.

80. Delorme A, Makeig S (2004) Eeglab: an open source toolbox for analysis of single-trial eeg dynamics including independent component analysis. *J. Neurosci. Methods* 134(1):9–21.

81. Oostenveld R, Fries P, Maris E, Schoffelen JM (2011) Fieldtrip: Open source software for advanced analysis of meg, eeg, and invasive electrophysiological data. *Comput. Intell. Neurosci.* 2011(1):1–9.

82. Komuro M, Kamiyama K, Endo T, Aihara K (2016) Quasi-periodic bifurcations of higher-dimensional tori. *Int. J. Bifur. Chaos* 26(7):1630016.

83. Lachaux JP, Rodriguez E, Martinerie J, Varela FJ (1999) Measuring phase synchrony in brain signals. *Hum. Brain Mapp.* 8(4):194–208.

84. He BJ, Zempel JM, Snyder AZ, Raichle ME (2010) The temporal structures and functional significance of scale-free brain activity. *Neuron* 66(3):353–369.

85. Su T, Dy JG (2004) A deterministic method for initializing k-means clustering in *Proc. 16th IEEE Int. Conf. Tools Artif. Intell.* pp. 784–786.

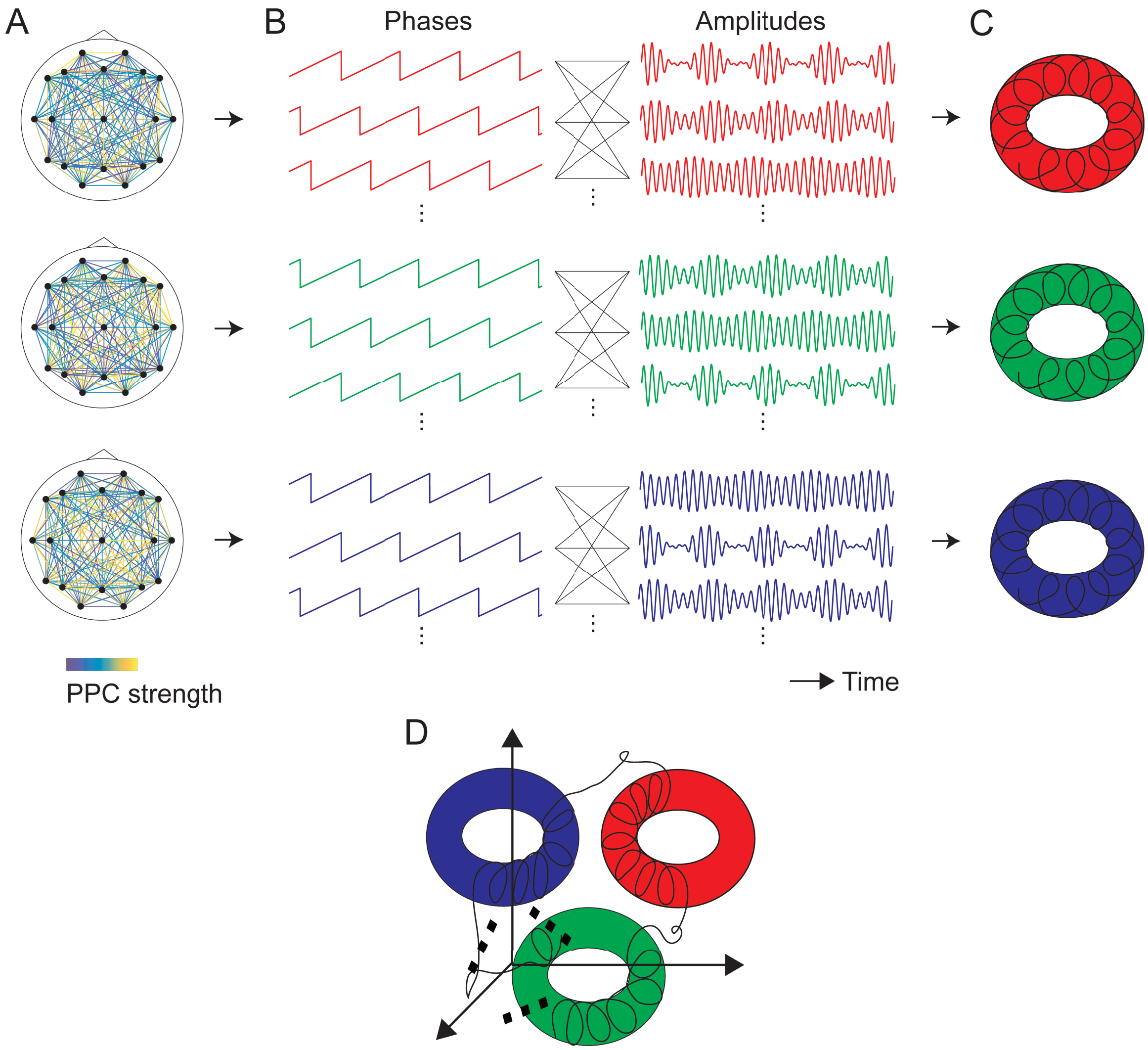

Figure 1. The dynamic PPC-PAC hypothesis. (A) A repertoire of synchronous slow oscillations that interact via the PPC; (B) slow oscillations that further interact with fast ones via the PAC; (C) the resulting possible attractors; and (D) transitions among the attractors. The dynamic PPC-PAC hypothesis states that for the resting brain, dynamic changes in PPC strengths (transitions among synchronous states (A)) can cause dynamic changes in PAC strengths because of PPC-PAC connectivity (B), and thereby yield transitions among oscillatory states with multiple peak frequencies (C and D). The oscillations of each state are quasi-periodic and their trajectory in the phase space can realize the transition to another state by spontaneous fluctuations in the brain; in other words, the underlying attractors can be tori and show metastability.

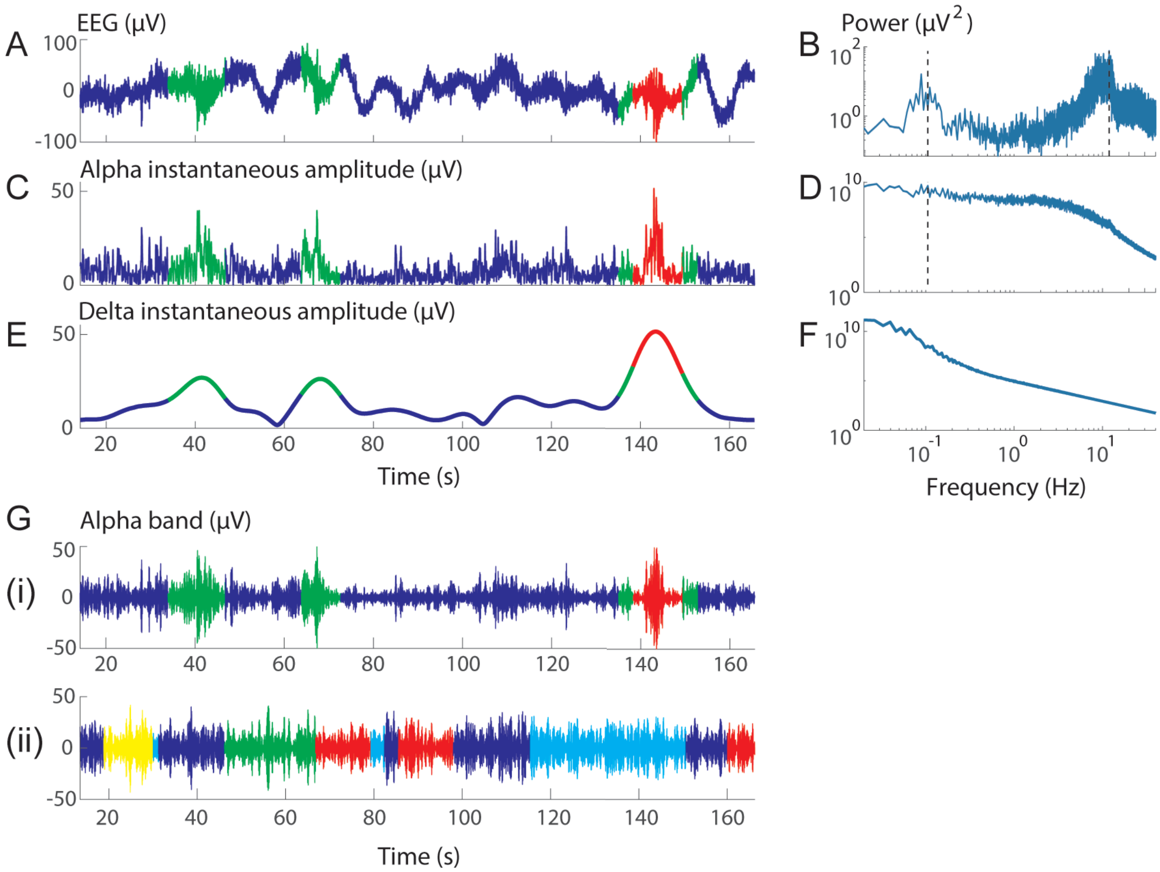

Figure 2. Dynamic changes in the delta-alpha PAC strength. (A) A representative raw EEG signal at the FC2 electrode, (C) the corresponding instantaneous amplitudes around an alpha-band peak frequency, and (E) those around a delta-band peak frequency (via two-time signal-to-instantaneous amplitudes conversions) with (B,D, and F) being corresponding power spectra. The alpha-band and delta-band peak frequencies were estimated from the single mean power spectrum of the raw EEG signals (B; Fig. S1) and the alpha-band instantaneous amplitudes (D), respectively, as depicted by the dotted lines in panels B and D. (G) The EEG alpha-band signal obtained from the same data (i), and another representative signal (ii) of faster transition among more states obtained from an individual with a lower AQ score (a signal at electrode POz). The colors in panels A, C, E, and G indicate distinct states.

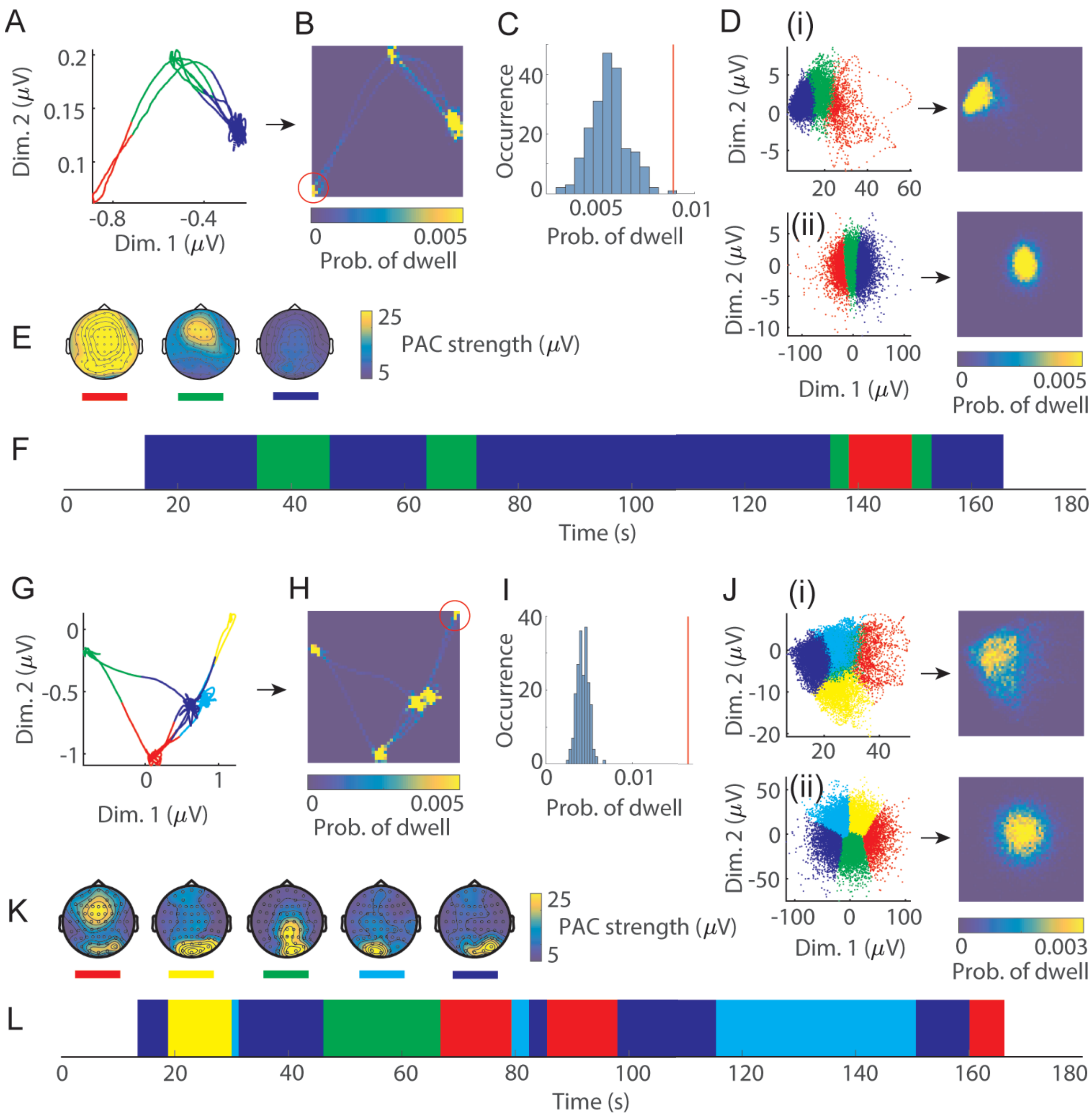

Figure 3. Transition dynamics among delta-alpha PAC states in a lower-dimensional space. (A to F) Representative delta-alpha PAC dynamics for an individual with higher attention-related AQ subscores (refer to Figs. 2A to 2G(i)) and an individual (G to L) with lower scores (refer to Fig. 2G(ii)). (A, G) The trajectory of labeled signals in a plane, (B, H) the corresponding bivariate histograms, and (C, I) surrogate data testing under a condition of $d = 2$. (D, J) Trajectories under conditions of $d = 1$ (i) and $d = 0$ (ii). (E, K) The resulting delta-alpha PAC states (mean PAC strengths) and (F, L) transitions among those states. Surrogate data testing was applied to the density of points indicated by the red circles in panels B and H and the red lines in panels C and I, and the null hypothesis H_0 was rejected for $d = 2$ (C and I); the surrogate data testing did not reject all individual datasets for $d = 1$ and many of them for $d = 0$ (for comparison purposes, refer to D and J in which the number of states is the same as $d = 2$). The delta-alpha PAC dynamics tended to stay in a state for a longer time and to visit a lower number of states in individuals with higher subscores for attention to detail and attention switching (compare F with L). The colors in panels A, F, G, and L indicate distinct states, as depicted in E and K.

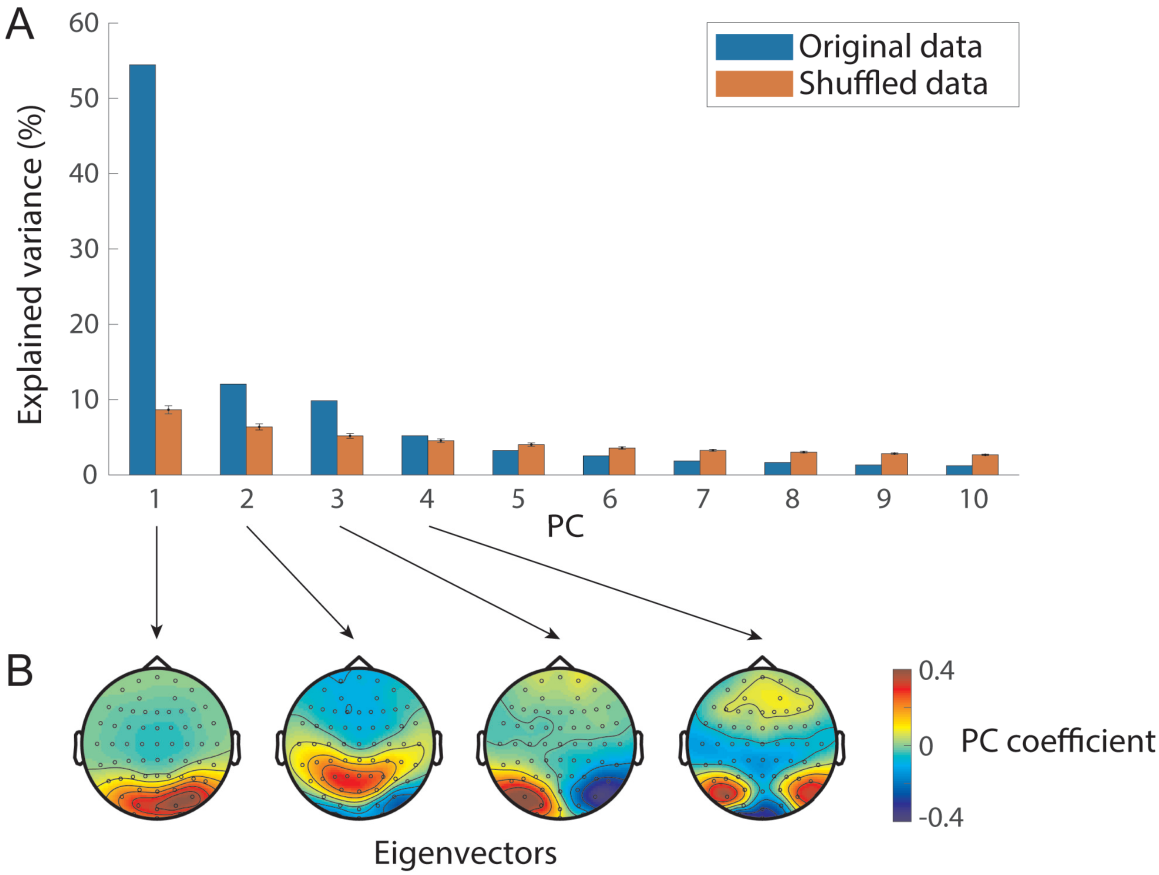

Figure 4. The four groups of consistent delta-alpha PAC states across individuals. (A) PCs of across-individual states and (B) eigenvectors of the first four PCs. The variance explained by the first four PCs was significant, and accounted for 81.6 % of total variance. The dataset used here was a set of the modified Z-scores of mean PAC strengths that were concatenated across states and individuals.

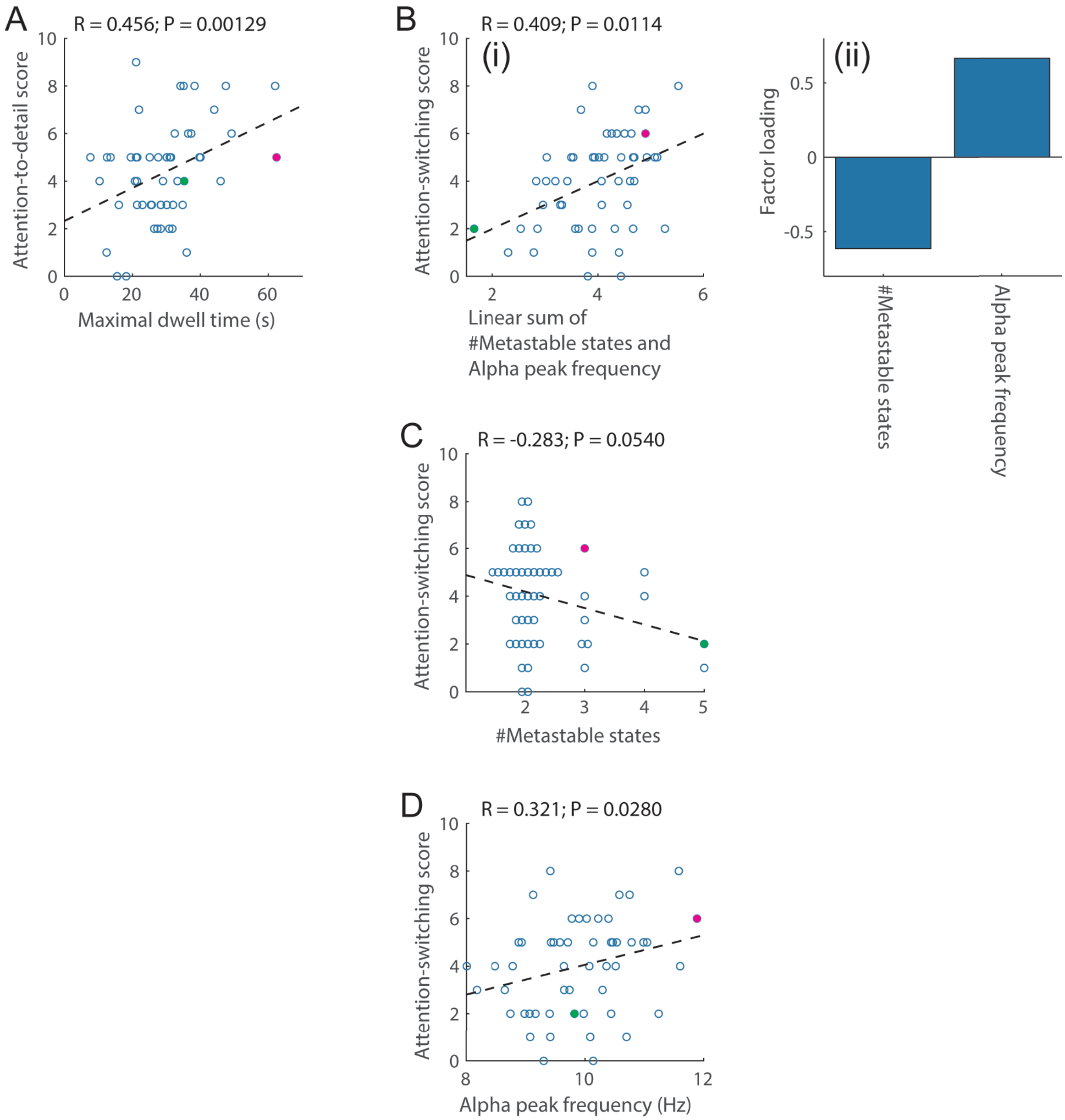

Figure 5. Correlations between delta-alpha PAC dynamics and attention-related AQ subscores. (A) Scatter plot of the attention-to-detail score against maximal dwell time. (B) Scatter plot of the attention-switching score against the linear sum of the number of states and the alpha-band peak frequency (i) with corresponding factor loadings (ii). (C, D) Scatter plots of the attention-switching score against the number of states and the alpha-band peak frequency, respectively. In each panel, the circles in magenta and green correspond to the representative individual delta-alpha PAC dynamics, as depicted in Figs. 3A to 3F and Figs. 3G to 3L, respectively. The dotted line in each panel indicates the fitted regression line.

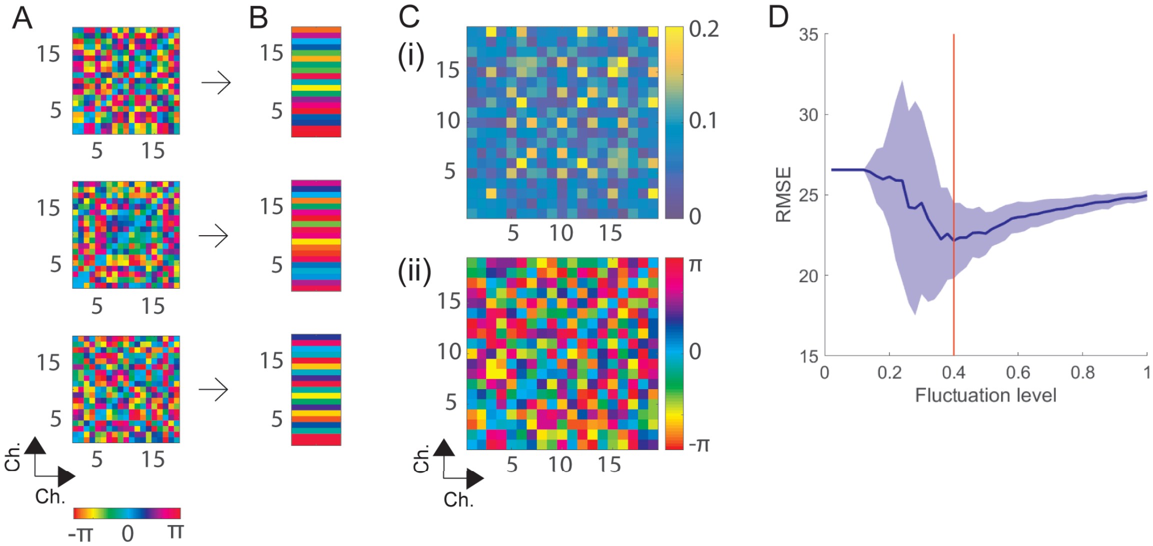

Figure 6. Estimation of PPC connectivity and the level of fluctuations from delta-band phase dynamics. (A) Mean phase lags between every pair of delta-band phases with respect to each delta-alpha PAC state, (B) the corresponding phases, (C) the estimated PPC connectivity as a complex-valued matrix with its absolute (i) and argument parts (ii), and (D) the estimated fluctuation level. The phases (B) combined with the Kuramoto model resulted in PPC connectivity (C), and the Kuramoto model with PPC connectivity was used for estimation of the fluctuation level (D). The data used in this Figure correspond to Figs. 2A to 2G(i) and Figs. 3A to 3F.

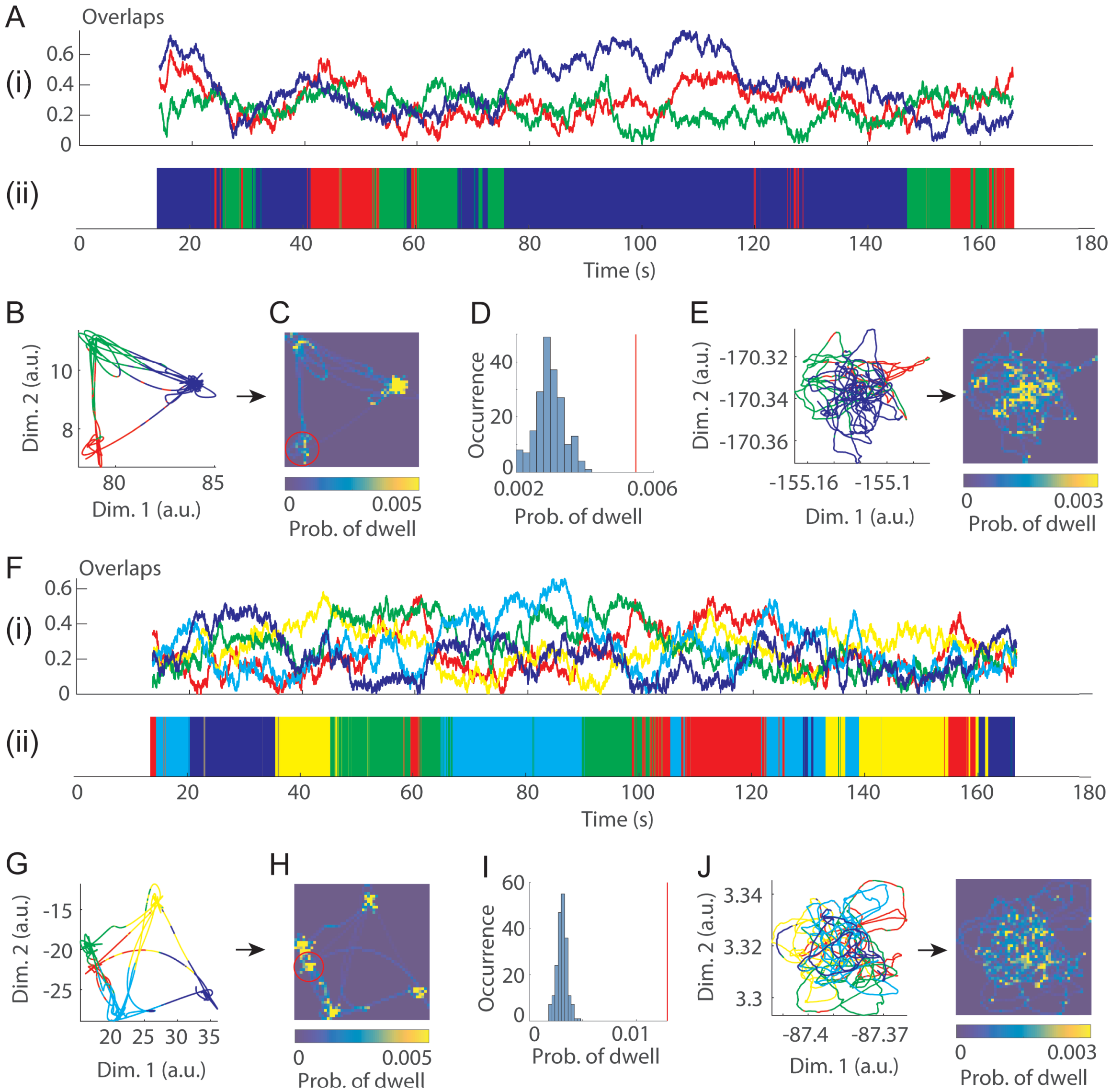

Figure 7. Simulation of delta-alpha PAC dynamics by a coupled oscillator system driven by spontaneous fluctuations. (A to E) The representative simulated delta-alpha PAC dynamics for an individual with higher attention-related AQ subscores (refer to Figs. 3A to 3F) and (G to L) those for an individual with lower scores (refer to Figs. 3G to 3L). (A, F) Time courses of overlaps (i) and the corresponding labels (ii) among delta-alpha PAC states. (B, G) The trajectory of labeled signals in a plane, (C, H) the corresponding bivariate histograms, and (D, I) surrogate data testing under condition $d = 2$. (E, J) The trajectory under condition $d = 1$. Surrogate data testing was applied to the density of points indicated by the red circles in panels C and H and the red lines in panels D and I, and the null hypothesis H_0 was rejected for $d = 2$ (D and I); it was not rejected for the condition $d = 1$. The model showed consistent results with the data analysis, evidence of the dynamic PPC-PAC hypothesis.

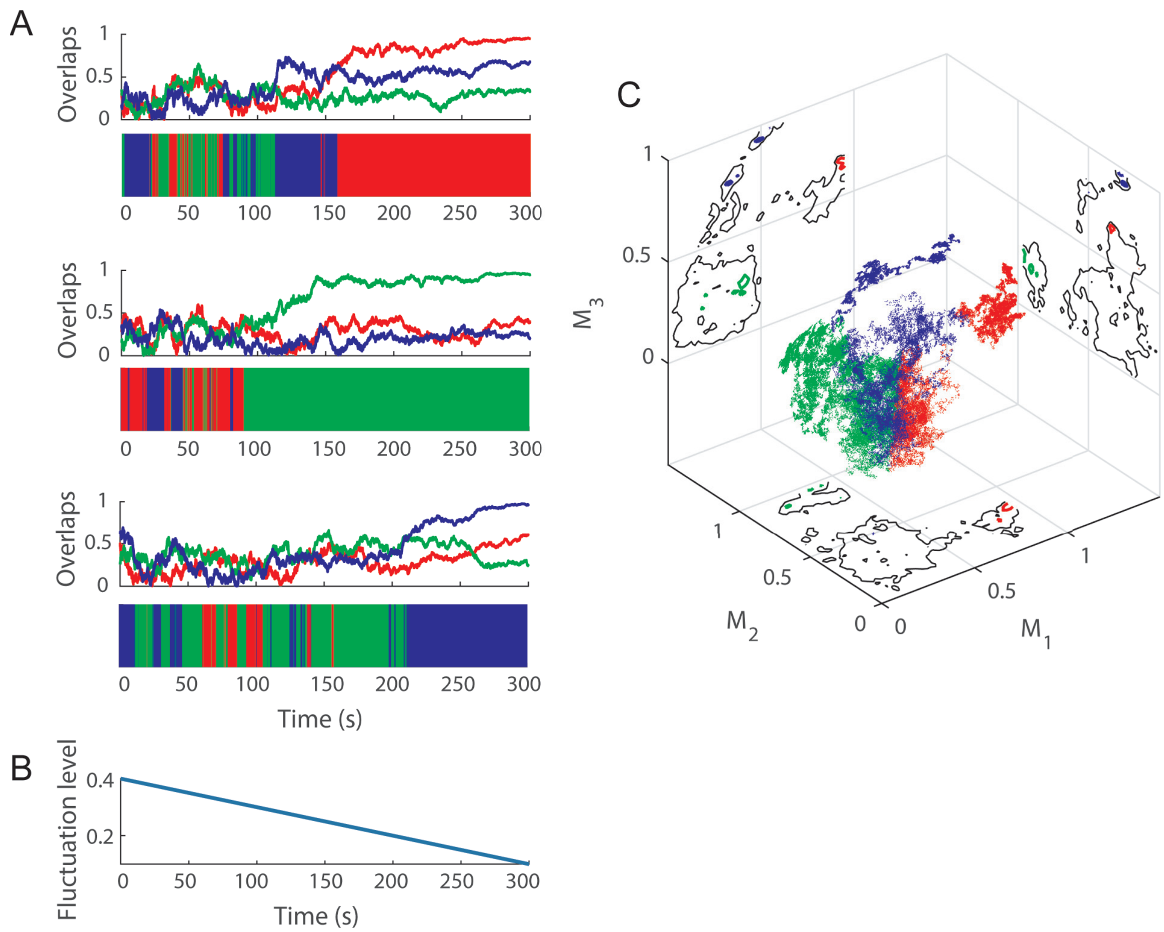

Figure 8. Shrinking of the simulated delta-alpha PAC dynamics with a temporally decreasing fluctuation level in the phase space: the qualitative change from the transition dynamics to the dynamics in a steady state. (A) Time courses of the overlaps with their labeled sequences under different initial conditions in cases where the dynamics can converge into one of three steady states; (B) the time course of the fluctuation level; and (C) the trajectories of overlaps in the phase space with their projections. The contour plots on projections in panel C indicate that the spaces filled by transition dynamics (black lines) can include the steady states (red, green, and blue lines) as their subsets. The data used in this Figure correspond to the individual with higher attention-related AQ subscores depicted in Figures 2A to 2G(i), 3A to 3F, 6 and 7A to 7E.